

Statistics of injected power on a bouncing ball subjected to a randomly vibrating piston

Alfredo García-Cid, Pablo Gutiérrez, Claudio Falcón, Sébastien Aumaître, Eric Falcon

▶ **To cite this version:**

Alfredo García-Cid, Pablo Gutiérrez, Claudio Falcón, Sébastien Aumaître, Eric Falcon. Statistics of injected power on a bouncing ball subjected to a randomly vibrating piston. Physical Review E , 2015, 92, pp.032915. 10.1103/PhysRevE.92.032915 . cea-01367017

HAL Id: cea-01367017

https://cea.hal.science/cea-01367017

Submitted on 15 Sep 2016

HAL is a multi-disciplinary open access archive for the deposit and dissemination of scientific research documents, whether they are published or not. The documents may come from teaching and research institutions in France or abroad, or from public or private research centers.

L'archive ouverte pluridisciplinaire **HAL**, est destinée au dépôt et à la diffusion de documents scientifiques de niveau recherche, publiés ou non, émanant des établissements d'enseignement et de recherche français ou étrangers, des laboratoires publics ou privés.

Statistics of injected power on a bouncing ball subjected to a randomly vibrating piston

Alfredo García-Cid, Pablo Gutiérrez, and Claudio Falcón*
Departamento de Física, Facultad de Ciencias Físicas y Matemáticas, Universidad de Chile, Casilla 487-3, Santiago, Chile

Sébastien Aumaître
Service de Physique de l'Etat Condensé, DSM, CEA-Saclay, UMR 3680 CNRS, 91191 Gif-sur-Yvette, France and Laboratoire de Physique, UMR-CNRS 5672, Ecole Normale Supérieure de Lyon, 46 allée d'Italie, Lyon, France

Eric Falcon
Univ Paris Diderot, Sorbonne Paris Cité, MSC, UMR 7057 CNRS, F-75 013 Paris, France
(Received 30 March 2015; published 29 September 2015)

We present an experimental study on the statistical properties of the injected power needed to maintain an inelastic ball bouncing constantly on a randomly accelerating piston in the presence of gravity. We compute the injected power at each collision of the ball with the moving piston by measuring the velocity of the piston and the force exerted on the piston by the ball. The probability density function of the injected power has its most probable value close to zero and displays two asymmetric exponential tails, depending on the restitution coefficient, the piston acceleration, and its frequency content. This distribution can be deduced from a simple model assuming quasi-Gaussian statistics for the force and velocity of the piston.

DOI: 10.1103/PhysRevE.92.032915 PACS number(s): 05.45.−a, 47.20.Ky

I. INTRODUCTION

Dissipative systems display striking dynamical behaviors when they are driven by an external forcing. A nonequilibrium steady state (NESS) can be achieved by balancing the effect of the external forcing and the inherent dissipative mechanisms of the system under study. In physics, the number of examples is vast. For instance, in fluid mechanics, a typical example of NESS is the so-called fully developed hydrodynamic turbulence [1,2], where the energy pumped at a large scales is transported towards small scales where it is dissipated by viscosity. In granular materials, a granular gas is a NESS achieved by injecting energy through the boundaries of a container into a dilute sample of particles which will later dissipate it via inelastic collisions, converting kinetic energy into plastic deformations [3–6]. Similar examples of nonequilibrium steady states can be found in electronic circuits [7–9], turbulent thermal convection [10], two-dimensional turbulence [11], wave turbulence in elastic plates [12] and surface waves [13], molecular machines [14], and so forth. In these steady states, the injected power or other global quantities (i.e., quantities averaged over space and/or time such as energy, momenta, and number of particles) will fluctuate strongly and depend on both the injection mechanism and the impedance of the system to the driving. Thus, in a NESS these global quantities cannot be regarded as constant as they depend on the interaction between the system and the injection mechanism, even in the case of time-periodic (sinusoidal) forcing [15]. When the driving can be described statistically by a Gaussian random process with zero mean, their fluctuations can be several times larger than their mean values [5,6,11–13]. It prevents the use of a large set of theoretical tools which are of fundamental use in the thermodynamical limit [16,17] which allow the prediction and control of systems with a large degree of components.

A simple example of how an out-of-equilibrium balance between injection and dissipation generates a NESS is an inelastic bouncing ball driven vertically by a randomly moving piston in the presence of gravity. In this simple system energy is pumped into the bouncing ball by the moving piston, which is dissipated mainly by plastic deformations of the bead and viscous drag with the air surrounding the ball. The dynamics of inelastic bouncing balls excited by vertical vibrations has been researched extensively theoretically, experimentally, and numerically as examples of permanent chaotic behavior when the piston moves periodically [18–21]. On the other hand, only a handful of theoretical studies have reported on the properties and features of the NESS dynamics of the inelastic bouncing ball system when the motion of the piston is quasiperiodic [22] or when the bead is subjected to a random acceleration [23]. It must be noticed that, experimentally, the injection of energy (or other quantities) into a dissipative system is usually accompanied by fluctuations, affecting the statistical properties of the NESS under study. Thus, an experimental study on the properties and features of the NESS achieved by a randomly excited inelastic bouncing ball is lacking.

In the present paper, we focus our work on the statistics of the injected power furnished by the randomly moving piston which is necessary to maintain an inelastic ball bouncing constantly. In Sec. II we present the experimental setup and measuring techniques used to quantify the injected power I_n on each impact of the bouncing ball. Section III shows the experimentally measured probability distribution functions (PDF) for the force F_n and velocity v_n of the moving piston as the bead makes the nth impact onto its surface, and with this data we compute the PDF of I_n. This distribution has its most probable value close to zero and displays two asymmetric exponential tails, depending on the restitution coefficient, the piston acceleration, and its frequency content. In Sec. IV we show that by using a simple modified bivariate distribution for F_n and v_n we can be compute theoretically the distribution of I_n. Finally, in Sec. V we discuss the possible applications of the model and how it can be generalized to granular gases.

*cfalcon@ing.uchile.cl

 ©2015 American Physical Society

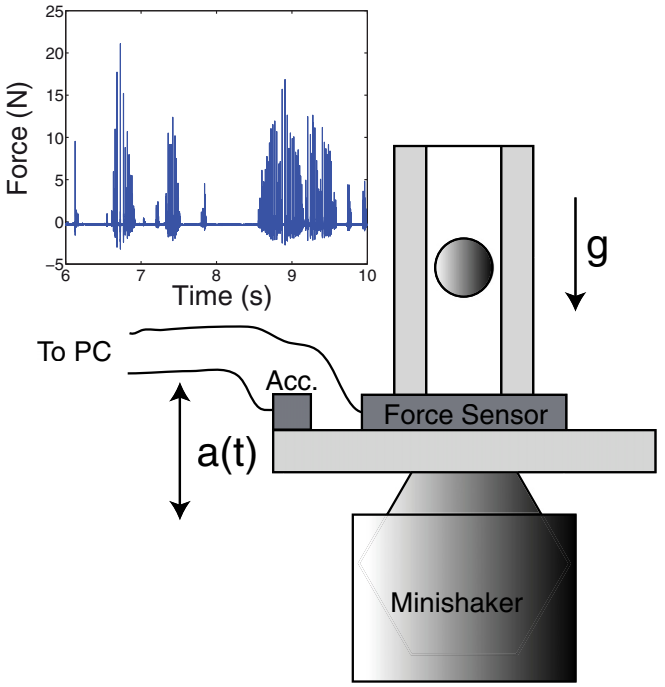


FIG. 1. (Color online) Experimental setup. Inset: Typical temporal trace of the force signal for a steel ball (ball mass $m = 8$ g, restitution coefficient $r = 0.923$) at a given control acceleration $\Gamma = 1.09$.

II. EXPERIMENTAL SETUP AND MEASUREMENT TECHNIQUES

The experimental setup is shown in Fig. 1. An 8 mm bead (made out of steel, brass, copper, polyurethane, or nylon, with ± 1 μm tolerance in diameter, ± 1 μm in sphericity with masses presented in Table I) is placed inside a vertical plexiglass enclosing tube (outer diameter 15 mm, inner diameter 9 mm), which is polished on its inside part to reduce sliding friction with the bead. The tube is screwed to a plexiglass piston driven randomly in time by a minishaker (B&K 4810). An accelerometer (B&K 4803) screwed to the oscillating piston measures the acceleration $a(t)$ of the whole setup via a charge amplifier (B&K 2635). The random forcing of the plexiglass piston, generated by a desktop computer using LabView via an acquisition card (NI-6022) through a power amplifier (B&K 2706), is a zero-mean colored Gaussian noise with a controlled frequency bandwidth $[f_l, f_u]$ and rms amplitude normalized with respect to gravity $\Gamma = \sqrt{\langle a(t)^2 \rangle}/g$. In our experiments f_u is fixed at 200 Hz. Thus, f_l and Γ serve as control parameters. At the bottom end of the tube a piezoelectric impact sensor (PCB-200B02) is attached to the oscillating piston, making impact with the bead. The impact signal is conditioned via a signal conditioner (PCB-480C02) for data treatment. From the acceleration signal, the velocity of the piston is computed by analog integration of the signal through the signal conditioner. Both force and acceleration signals are digitally acquired at 750 kHz, numerically low-passed filtered at 50 kHz to avoid the electrical resonance of the force sensor at 70 kHz, and stored in the desktop computer.

TABLE I. Masses and COR for different materials using spheres of 8 mm in diameter. The COR with and without confinement are r_c and r, respectively.

Material	m (g)	r_c	r
Steel	2.053 ± 0.010	0.770 ± 0.011	0.923 ± 0.006
Bronze	2.235 ± 0.033	0.746 ± 0.012	0.861 ± 0.028
Brass	2.383 ± 0.005	0.742 ± 0.036	0.860 ± 0.015
Nylon	0.295 ± 0.006	0.757 ± 0.011	0.740 ± 0.042
Polyurethane	0.308 ± 0.008	0.634 ± 0.024	0.667 ± 0.029

A. Coefficient of restitution r

In order to understand the dissipative motion of an inelastic bead bouncing on a randomly moving piston, we first measure the experimental coefficient of restitution (COR) r for different beads of different materials following a scheme similar to the one proposed in Ref. [24]. To do this, the impact sensor is screwed on an aluminum block ($10 \times 20 \times 4$ cm^3), on top of which an aluminum tube (outer diameter 20 mm, inner diameter 15 mm) is placed. A micrometric screw holds the bead inside the tube at a height $h_o = 5$ mm over the impact sensor, allowing a controlled release of the bead with almost negligible air entrainment. The initial impact velocity v_o coming from the free falling of the bead can be estimated $v_o = \sqrt{2h_o g} \simeq 30$ cm/s. Horizontal and rotational velocities are also negligible for this experimental configuration.

r is defined as the ratio between the bead velocity before and after an impact and it is assumed to be constant [24]. Thus, the COR can be computed as $r = v_{n+1}/v_n$. The measurement of v_n and v_{n+1} is difficult, but we can compute its ratio using simple particle mechanics relating r with the time of flight of the particle.

B. Calculation of r via time of flight

The total time elapsed d_n between the nth and $n+1$th impact can be measured from the series of force peaks (as the one shown in Fig. 2), which can be used to compute r. d_n can be expressed as $d_n = \tau_n + t_n$, where τ_n is the duration of the nth collision and t_n is the time of flight in between shocks. These times are measured from the temporal trace of the impact sensor, which consists of a series of peaks showing the time events where the bead impacts the sensor bouncing repeatedly over the piston in shortening time intervals as shown in Fig. 3.

Assuming negligible dissipation in between these intervals the ball is performing parabolic flights lasting t_n. d_n is computed as the temporal difference between two consecutive maxima of the force signal (discriminating between the real maxima and those arising from the piezoelectric inertial oscillation with a temporal period ~ 100 μs). τ_n is computed as the temporal width of the impact curve (which is always smaller than $\sim$ 100 μs). Thus, $\tau_n \ll t_n$ and $d_n \simeq t_n$. We compute the COR from the set of t_n using point particle dynamics [24]:

$$t_n = r \times t_{n-1} = r^n \times \sqrt{\frac{8h_o}{g}}. \quad (1)$$

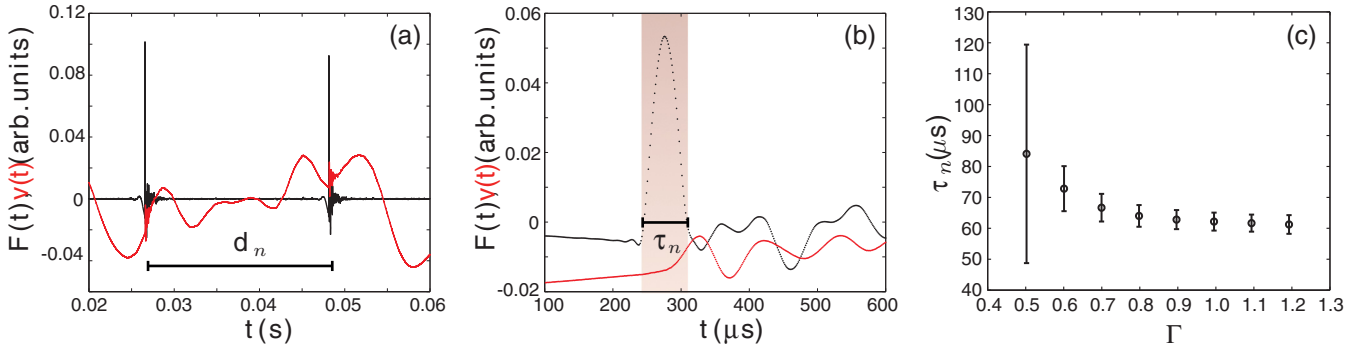


FIG. 2. (Color online) (a) Temporal traces for the force (black) and velocity (red) traces between two impacts, defining d_n for $\Gamma = 1.09$. (b) Temporal traces for the force (black) and velocity (red) traces, around an impact for $\Gamma = 1.1$. The shaded region defines τ_n. Arbitrary units are used to place both curves in the same scale. (c) Dependence of τ_n as a function of Γ. Error bars stand for the standard deviation for τ_n. The bead is made of steel.

C. Dissipation effects

As stated above, in this approximation, no viscous drag, sliding friction, or velocity-dependent effects on r are taken into account. Taking the natural logarithm on both sides we compute r as the slope of $\log t_n$ versus n, as is shown in Fig. 3. r is defined as the mean slope of five different trials. This procedure was used to compute the COR for five different materials, as presented in Table I. The COR was also measured following the same scheme but using the enclosing tube to constrain the bead horizontal dynamics. This shifts r values to lower ones, as air entrainment becomes important and even dominant in the bead dynamics. Values for the COR with (r_c) and without confinement (r) are shown also in Table I.

The difference between r and r_c appears as a combination of the effect of air entrainment and wall friction due to confinement, affecting the measurement of the COR as the initial and terminal velocity after a bounce of the inelastic ball. In the literature, the problem of the terminal speed change due to confinement (which is responsible for the shift to lower values of r) has been extensively studied for different tube and particle diameters, terminal speeds, confinement fluids, and flow regimes (see Ref. [25] and references therein). Thus, we will work using the effective r_c in what follows and leave this effect for future studies.

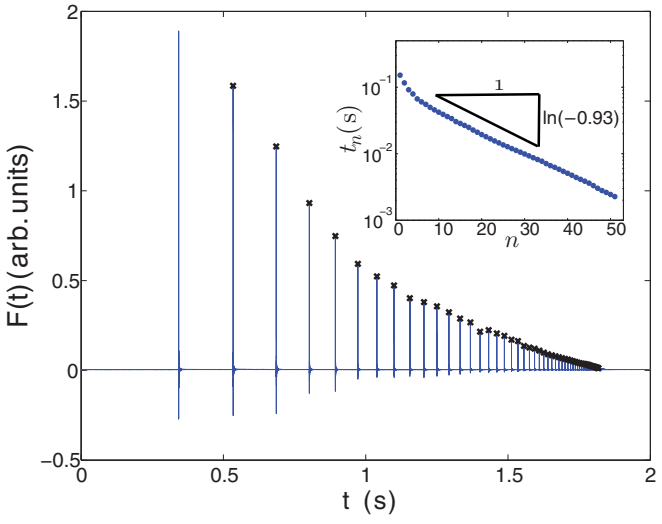


FIG. 3. (Color online) Typical trace of force impacts of a steel ball on a piston on repose. Symbols (×) stand for peak detections. Inset: Semilog plot of time lag between impacts t_n vs n for a steel ball. Best fitting slope is ln(−0.93).

In Fig. 2 we show how d_n and τ_n are defined from the acquired temporal traces. The values of d_n change as piston moves, but its typical scale is still much larger than τ_n. The values of τ_n change slightly depending on Γ: τ_n is of the order of 50 μs when the piston is in repose and 65 μs when the piston is moving randomly. These differences are taken into account when computing the discrete values of the exerted force and velocity of the piston, as is shown below.

III. EXPERIMENTAL RESULTS

As shown in Fig. 2, a typical trace of the force and velocity for a steel bead ($r_c = 0.770$, $\Gamma = 1.09$, $f_l = 0$) displays peaks and oscillations. The force signal consists of a series of peaks separated by the randomly spaced time intervals t_n (as explained above). Between these intervals, the ball performs parabolic flights inside the tube. On the other hand, the velocity signal of the piston randomly fluctuates around zero. Around each impact n, we compute the discrete force F_n and velocity v_n by integrating the force and velocity signals in the time interval τ_n. Each experimental run lasts 100 s. Between 10 and 500 collisions are observed, depending on the control parameters. To obtain sufficient data points for statistical analysis of all values of the control parameters ($\sim 5 \times 10^4$), 100 runs are done for each value of these parameters.

A. Statistics of F_n and v_n as a function of Γ

Let us begin by studying the statistics of F_n as a function of Γ shown in Fig. 4. There is a transition from an exponential to a convexly shaped PDF with increasing Γ. All the moments of F_n increase with increasing Γ. For large Γ the PDF of F_n can be fitted accurately by a Gaussian curve with only positive events almost centered at $F_n = 0$. This effect can be better observed in the normalized PDFs for the rescaled variable $F_n/\sigma(F_n)$, displayed in the inset of Fig. 4 (top), where a Gaussian fit is plotted (although the fit is not a normalized Gaussian with standard deviation equal to unity). The bottom of Fig. 4 shows the statistics for v_n as a function of Γ. All the curves can be accurately fitted by a Gaussian curve centered at $v_n = 0$

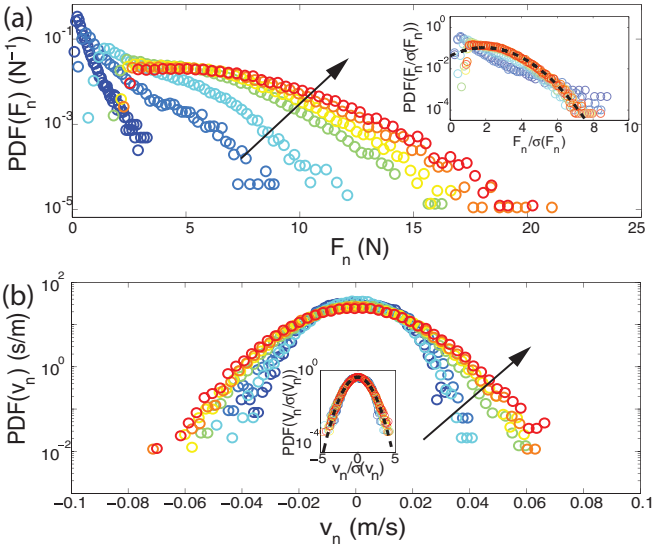


FIG. 4. (Color online) (a) PDF for F_n for $\Gamma = 0.50$, 0.60, 0.68, 0.80, 0.87, 1.0, 1.09, and 1.28 for steel ($r_c = 0.770$) and $f_l = 0$ Hz. Inset: PDF of the normalized variable $F_n/\sigma(F_n)$ for $\Gamma = 0.50$, 0.60, 0.68, 0.80, 0.87, 1.00, and 1.09 for steel ($r_c = 0.770$) and $f_l = 0$ Hz. (b) PDF of v_n for $\Gamma = 0.50$, 0.60, 0.68, 0.80, 0.87, 1.0, and 1.09 for steel ($r_c = 0.770$) and $f_l = 0$ Hz. Inset: PDF of the normalized variable $v_n/\sigma(v_n)$ for $\Gamma = 0.50$, 0.60, 0.68, 0.80, 0.87, 1.0, 1.09, and 1.28 for steel ($r_c = 0.770$) and $f_l = 0$ Hz. Dashed line is a normalized Gaussian. Arrows indicate how Γ increases.

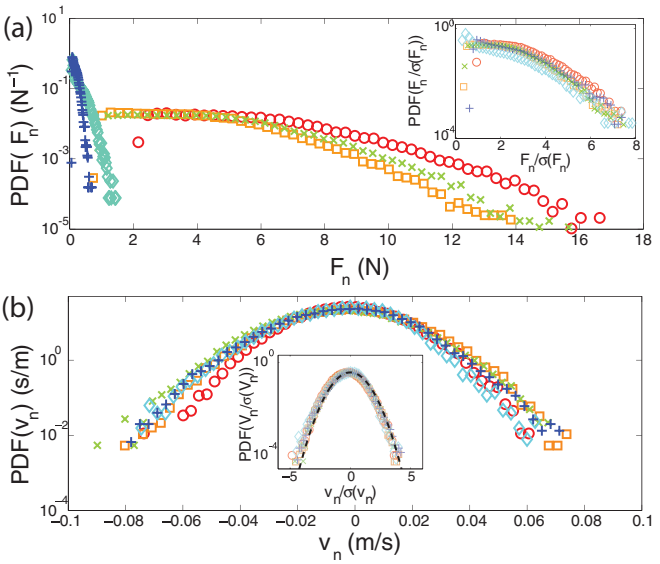


FIG. 5. (Color online) (a) PDF for F_n for steel ($\circ$), brass ($\times$), bronze ($\square$), nylon ($\diamond$), and polyurethane ($+$) for $\Gamma = 1.00$ and $f_l = 0$ Hz. Inset: PDF for the normalized variable $F_n/\sigma(F_n)$ for steel ($\circ$), brass ($\times$), bronze ($\square$), nylon ($\diamond$), and polyurethane ($+$) for $\Gamma = 1.00$ and $f_l = 0$ Hz. (b) PDF for v_n for steel ($\circ$), brass ($\times$), bronze ($\square$), nylon ($\diamond$), and polyurethane ($+$) for $\Gamma = 1.00$ and $f_l = 0$ Hz. Inset: PDF for the normalized variable $v_n/\sigma(v_n)$ for steel ($\circ$), brass ($\times$), bronze ($\square$), nylon ($\diamond$), and polyurethane ($+$) for $\Gamma = 1.00$ and $f_l = 0$ Hz.

with a standard deviation growing linearly with Γ. As for F_n, this effect can be better observed in the normalized PDFs for the rescaled variable $v_n/\sigma(v_n)$ shown in the inset of Fig. 4 (bottom), where a normalized Gaussian curve is plotted to emphasize this dependence.

B. Statistics of F_n and v_n as a function of r_c

Fixing now Γ at 1.00 and $f_l = 0$ Hz, we change the bead material. Five different materials were used with different values of r_c (see Table I). The PDFs of F_n for different values of r are shown in Fig. 5 (top). A large difference between metallic and plastic beads is found in the typical values of F_n. The rms value of metallic beads is 10 times larger than the one for plastic ones. In the normalized variable $F_n/\sigma(F_n)$, the PDFs do not collapse on the same curve [see inset of Fig. 5 (top)]. The order of the curves is nonmonotonic with r_c. The PDFs of v_n for different values of r_c are shown in Fig. 5 (bottom). The different curves are very similar in scale and shape. A slight asymmetry towards positive values of v_n can be observed on the curves when plotted in the rescaled variable $v_n/\sigma(v_n)$ [see Fig. 5 (bottom)], as can be seen when compared to a normalized Gaussian curve.

C. Statistics of F_n and v_n as a function of f_l

Fixing now Γ at 1.00 and using a brass bead ($r_c = 0.742$), we change the low-frequency cutoff f_l from 0 to 150 Hz. The PDFs of F_n for different values of f_l are shown in Fig. 6 (top). As f_l increases, the typical rms fluctuations of F_n decrease and new local maxima appear in the PDFs. These maxima are related to the appearance of a pseudoperiodic motion of the bead as the bandwidth of the forcing becomes narrower around 200 Hz (the upper cutoff frequency of the selected bandwidth). When plotted in the rescaled variable $F_n/\sigma(F_n)$, the curves

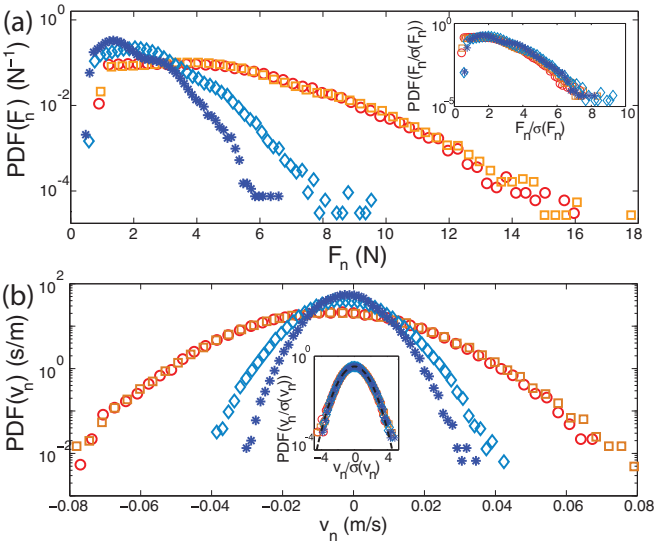


FIG. 6. (Color online) (a) PDF for F_n for $f_l = 0$ ($\circ$), 50 ($\square$), 100 ($\diamond$), and 150 ($*$) Hz for $\Gamma = 1.00$, and $r_c = 0.742$ (brass). Inset: PDF for the normalized variable $F_n/\sigma(F_n)$ for $f_l = 0$ ($\circ$), 50 ($\square$), 100 ($\diamond$), and 150 ($*$) Hz for $\Gamma = 1.00$ and $r_c = 0.742$ (brass). (b) PDF for v_n for $f_l = 0$ ($\circ$), 50 ($\square$), 100 ($\diamond$), and 150 ($*$) Hz for $\Gamma = 1.00$ and $r_c = 0.742$ (brass). Inset: PDF for the normalized variable $v_n/\sigma(v_n)$ for $f_l = 0$ ($\circ$), 50 ($\square$), 100 ($\diamond$), and 150 ($*$) Hz for $\Gamma = 1.00$ and $r_c = 0.742$ (brass).

present a great level of collapse, although not complete. The PDFs of v_n for different values of f_l are shown in Fig. 6 (bottom). They are similar in shape, and their respective rms fluctuations decrease with increasing f_l. A slight asymmetry can be observed on the curves when plotted in the rescaled variable $v_n/\sigma(v_n)$ [see Fig. 6 (bottom)], as can be seen when compared to a normalized Gaussian curve.

D. Injected power I_n statistics as a function of Γ, r, and f_l

Using the discrete force F_n exerted by the piston on the bead and velocity v_n of the piston, we can compute the discrete power $I_n = F_n \times v_n$ injected on the bouncing bead system by the piston as a function of the nondimensional rms acceleration Γ, the COR r_c and the lower cutoff frequency f_l, as is shown in Fig. 7. Following the scheme presented above, we first fixed $r_c = 0.770$ and $f_l = 200$ Hz, and we computed

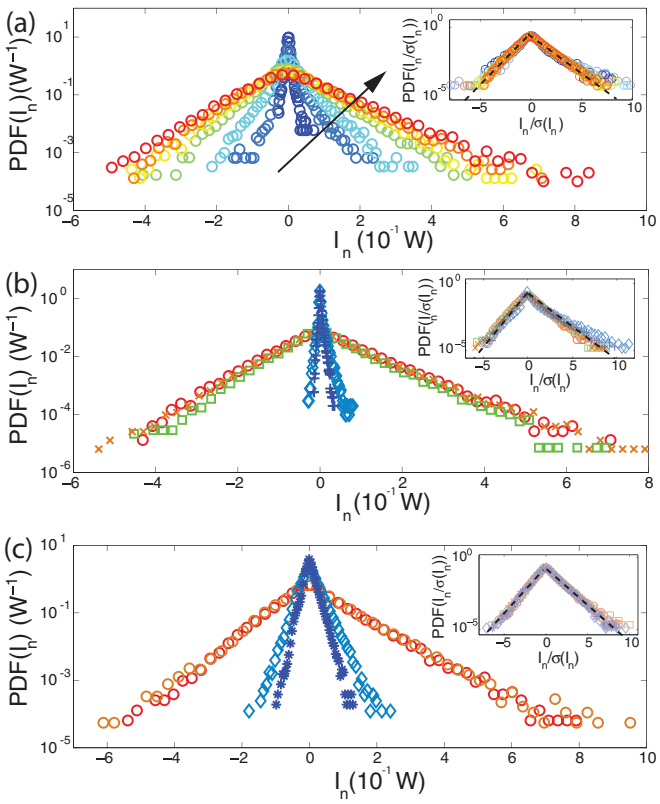


FIG. 7. (Color online) (a) PDF for I_n for $\Gamma = 0.50$, 0.60, 0.68, 0.80, 0.87, 1.00, and 1.09 for steel ($r_c = 0.770$) and $f_l = 0$ Hz. Inset: PDF of the normalized variable $I_n/\sigma(I_n)$ for $\Gamma = 0.50$, 0.60, 0.68, 0.80, 0.87, 1.00, and 1.09 for steel ($r_c = 0.770$) and $f_l = 0$ Hz. Dashed lines are exponential fits for both positive and negative tails. (b) PDF for I_n for steel ($\circ$), brass ($\times$), bronze ($\square$), nylon ($\diamond$), and polyurethane ($+$) for $\Gamma = 1.00$ and $f_l = 0$ Hz. Inset: PDF for the normalized variable $I_n/\sigma(I_n)$ for steel ($\circ$), brass ($\times$), bronze ($\square$), nylon ($\diamond$), and polyurethane ($+$) for $\Gamma = 1.00$ and $f_l = 0$ Hz. Dashed lines are exponential fits for both positive and negative tails. (c) PDF for I_n for $f_l = 0$ ($\circ$), 50 ($\square$), 100 ($\diamond$), and 150 ($*$) Hz for $\Gamma = 1.00$ and $r_c = 0.742$ (brass). Inset: PDF for the normalized variable $I_n/\sigma(I_n)$ for $f_l = 0$ ($\circ$), 50 ($\square$), 100 ($\diamond$), and 150 ($*$) Hz for $\Gamma = 1.00$ and $r_c = 0.742$ (brass). Dashed lines are exponential fits for both positive and negative tails.

the statistics of I_n by changing Γ. The PDFs display a cusp center at $I_n = 0$ and tails which are asymmetrical; i.e., the probability of finding positive injected power events ($I_n > 0$) is larger than the probability of finding negative injected power events ($I_n < 0$). This means that the mean injected power $\langle I_n \rangle$ is positive for every experimental run, which is needed in out-of-equilibrium systems as power will later be dissipated by internal mechanisms. For very low values of Γ, the tails decrease slower than an exponential (the convexity of the slopes is positive). As Γ increases the slopes become exponential and the typical scale of the fluctuations of I_n increases. In the rescaled variable $I_n/\sigma(I_n)$ the curves collapse into a master curve which displays exponential tails. When we fix $\Gamma = 1.00$ and $f_l = 200$ Hz and we change r_c, the PDFs of I_n display a large difference between metallic and plastic beads (as in the case for F_n). The rms value of I_n for metallic beads is 10 times larger than the one for plastic ones. In the normalized variable $I_n/\sigma(I_n)$, the PDFs collapse on the same curve [see inset of Fig. 7 (top)], displaying asymmetric exponential tails and a cusp close to $I_n = 0$. Fixing Γ at 1.00 and r_c at 0.742, we change f_l from 0 to 150 Hz. As before, the PDFs of I_n for different values of r_c are similar in shape, and their respective rms fluctuations decrease with increasing f_l. In the rescaled variable $I_n/\sigma(I_n)$ all curves collapse into the same master curve, which displays exponential asymmetric tails.

In computing I_n we have used the discrete multiplication instead of the integral over the collision time τ_n of the product of force and velocity. The statistics of either computation method are almost equal, except for $\Gamma < 0.6$ where the cusp near I_n is rounder and smaller. This means that the approximation of I_n as the direct multiplication of F_n and v_n is a valid choice. In this framework, the features of this PDF can be understood, as is shown in the next section.

IV. FEATURES OF THE INJECTED POWER STATISTICS

A way to understand the qualitative features of the PDF of injected power is to adapt the simple model proposed in Ref. [13] following Craig's XY distribution [26]. From the acquired data, we can see that the fluctuations of v_n can be described accurately by a Gaussian random variable with zero mean. The fluctuations of F_n cannot be described as the fluctuations of v_n, as no negative values of F_n can be achieved, even though the positive F_n events are well fitted by a Gaussian curve. Thus, from the data presented above, F_n can be approximated a semi-Gaussian variable, i.e., a random variable whose PDF is the product of a Gaussian and a Heaviside function (suitably normalized). We can model the PDF of F_n, $P(F_n)$ as

$$P(F_n) = \begin{cases} \sqrt{\frac{2}{\pi}}\frac{1}{\alpha}\exp\left(-F_n^2/2\alpha^2\right), & \text{for } F_n \geqslant 0. \\ 0, & \text{otherwise.} \end{cases} \quad (2)$$

where α is the standard deviation of the Gaussian function if no restriction for negative values of F_n is in place. Using the approximation that the exerted force per impact F_n drives the inelastic bead into motion, while it changes the momentum of the piston, we calculate the injected power $I_n = F_n \times v_n$ (even in this case where F_n is always positive). Here the injected power into the bouncing ball system is computed by

the multiplication of the velocity and force of the piston, as in Ref. [13]. The PDF of I_n can be derived from direct integration of the joint probability distribution function for F_n and v_n with suitable integration domains.

Let us use a simple model to compute the PDF of I_n. In the case of two Gaussian variables which are correlated (linear statistical dependence), the joint probability distribution function is a bivariate distribution

$$P(F_n,v_n)=\frac{\exp\left\{-\frac{1}{2(1-c^2)}\left[\frac{v_n^2}{\sigma(v_n)^2}-\frac{2cv_nF_n}{\sigma(F_n)\sigma(v_n)}+\frac{F_n^2}{\sigma(F_n)^2}\right]\right\}}{2\pi\sigma(v_n)\sigma(F_n)\sqrt{1-c^2}}, \tag{3}$$

where $c=\frac{\langle(F_n-\langle F_n\rangle)(v_n-\langle v_n\rangle)\rangle}{\sigma(F_n)\sigma(v_n)}$ is the correlation coefficient for the pair of random variables (F_n,v_n). Although other joint distribution functions can be displayed for two Gaussian variables with a given correlation [27], we model our system with this joint distribution because of its simplicity in the calculation of the PDF of I_n. Changing variables to $I_n=F_n\times v_n$ and $u_n=F_n$ and integrating Eq. (3) over F_n on the domain $[-\infty,\infty]$ we obtain the PDF for I_n:

$$P(I_n)=\frac{\exp\left[\frac{cI_n}{(1-c^2)\sigma(F_n)\sigma(v_n)}\right]}{\pi\sigma(F_n)\sigma(v_n)\sqrt{1-c^2}}K_o\left[\frac{|I_n|}{(1-c^2)\sigma(F_n)\sigma(v_n)}\right], \tag{4}$$

where $K_o(\cdot)$ is the zeroth order modified Bessel function of the second kind. A simple expression of the above equation can be achieved by the steepest descent method,

$$P(\hat{X})\sim\exp(c\hat{X}-|\hat{X}|)/\sqrt{|\hat{X}|}, \tag{5}$$

with $\hat{X}=I_n/[(1-c^2)\sigma(F_n)\sigma(v_n)]$. In addition $\langle I_n\rangle=\langle F_n\times v_n\rangle=c\times\sigma(F_n)\sigma(v_n)$, which connects the correlation coefficient of both variables, their rms fluctuations, and the injected power into the system. This expression displays two exponential tails controlled solely by the correlation coefficient c, which is equal to the mean injected power normalized when $\langle v_n\rangle=0$.

We can obtain an expression for the PDF of I_n by assuming that F_n is semi-Gaussian and integrating it out in Eq. (3). The new PDF for I_n has the same form as Eq. (4) with two modifications: by direct computation $\langle F_n\rangle=\sqrt{2/\pi}\alpha$ and $\sigma(F_n)=\alpha^2(1-2\pi)$, which are functions of α. With these substitutions in Eq. (3), the calculation of $P(I_n)$ is the same as the one above. To wit, we plot in Fig. 8 the PDFs of I_n in the reduced variable $X/(1-\langle X\rangle^2)$ with $X=I_n\sqrt{1-2/\pi}/[\sigma(F_n)\sigma(v_n)]$ and the theoretical approximation for its PDF following Eq. (5). There is a good agreement for every COR between experimental and theoretically predicted curves. As predicted, the approximation to the theoretical PDF is good, although the negative tails depart from the predicted slope slightly for polyurethane. Notice that Eq. (4) uses no fitting parameters: all cumulants of X can be computed by knowing c.

V. DISCUSSION AND CONCLUSIONS

The discrete injected power I_n needed to drive an inelastic bead into a NESS is studied. Power is injected via a randomly accelerating piston that drives the motion of the bead. Measuring both the mean force exerted by the piston over the inelastic bead and the mean velocity of the piston at each impact we can access the complete statistics of I_n. We showed that by changing the rms fluctuations and frequency band of the random acceleration, and the restitution coefficient of the bead, the typical scale of the fluctuations of I_n can change drastically, although the shape of the PDF of I_n does not, as it is controlled solely by the normalized injected power $c=\langle(F_n-\langle F_n\rangle)(v_n-\langle v_n\rangle)\rangle/\sigma(F_n)\sigma(v_n)$. Using a simple model stemming from a bivariate distribution function the PDF can be predicted only knowing c, $\sigma(v_n)$, and $\sigma(F_n)$. This is shown in Fig. 8: as r_c is similar for four out of five materials used in the experiment, the PDFs of the normalized injected power display the same shape for a given Γ and f_l and only for the case of polyurethane ($r_c=0.634$) shows a large deviation from the other curves. Thus, in this simple out-of-equilibrium case, one can predict and compute the PDF of I_n with only a very small set of external parameters which control completely the injected power statistics into an out-of-equilibrium system.

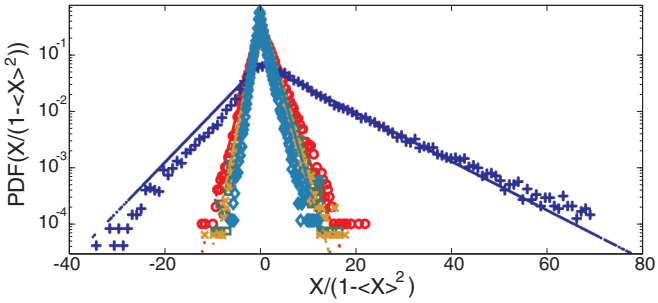


FIG. 8. (Color online) PDF of the reduced variable $X/(1-\langle X\rangle^2)$ with $X=I_n\sqrt{1-2/\pi}/[\sigma(F_n)\sigma(v_n)]$ for steel (○), brass (×), bronze (□), nylon (◇), and polyurethane (+) for $\Gamma=1.00$ and $f_l=0$ Hz. Dots show the approximation $P(X)\sim\exp(cX-|X|)/\sqrt{|X|}$ for each value of r_c.

The PDFs exhibited in Fig. 8 are actually quite generic of the injected power furnished by a random force. The simplest system of this type is a single particle submitted to a viscous drag and a random external force. This system can be described as an Ornstein-Uhlenbeck random process (a noise with exponential correlation [16,17]). In the case using the joint bivariate normal probability function (3), the PDF of the injected power can be computed exactly [28]. Experimentally, such PDFs have been observed for a randomly vibrated thin elastic plate [12] as well as in randomly forced surface waves [13]. The shape of these PDFs can be also achieved in turbulent shell model submitted to random force [28]. This kind of fluctuations can be observed for other quantities resulting from the product of two centered random variables. The components of the turbulent Reynold stress tensor [29] or the rate of transferred energy in turbulence [30] displays the same features. They also appear in turbulent convection for the local heat transfer, which is mainly the product of temperature and vertical velocity fluctuations. Asymmetric PDFs with a cusp near zero and exponential tails were observed for the temporal fluctuations of the locally measured heat flux [31], for the instantaneous fluctuations in space of the numerically computed heat flux [32], and for the measurement of the heat flux using a Lagrangian probe [33]. There may exist

other situations where such fluctuations are displayed. Even if the two variables involve in the product are not necessary Gaussian, the expression for the PDF of the injected power (4) is a useful benchmark to study the fluctuations of such a product. Thus, this simple yet powerful approach to the global fluctuations of an out-of-equilibrium system used in other NESS [8,11–13] serves as a tool to study the statistical properties of different systems.

In that sense, the use of this approach can be thought as an opportunity to rethink the pertinence of some of the tools of out-of-equilibrium fluctuations, for instance, fluctuation theorems [34], which are used to compute parameters associated to dissipative constants and effective energy scales (as in the case of the granular temperature [5,6]). Our work shows that from the statistics of I_n we can distinguish what would be an effective dissipation coefficient in a dissipative out-of-equilibrium system. In our experiments, the different masses of the beads do not affect the PDF of the reduced variable X, even when the difference is one order of magnitude in mass. Only the different values of r_c (which in our case depends on geometrical factors, viscous drag, friction, and plasticity of the material) affect the measured statistics of X as is shown in Fig. 8. Thus, r_c is a relevant control parameter of the dissipative system as it controls the amount of power that can be injected into the bouncing bead. The idea of the construction of an effective dissipation coefficient in dissipative out-of-equilibrium systems (such as the case of r_c) can thus be exported to systems where internal dissipative mechanisms are not yet measured or not well understood. Simple models for the statistics of the injected power, as the one presented here or elsewhere [28], can be used to quantify, for instance, typical dissipative scale differences between systems as internal parameters are changed, even though no complete information of the internal microscopic dynamics is known. The application of this scheme on other dissipative out-of-equilibrium systems is then needed to confirm its potential use.

ACKNOWLEDGMENTS

C.F. thanks Univ Paris Diderot for their Invited Researcher funding in Paris. E.F. thanks Ecos-Chili ECOS C07E07 for their Invited Researcher funding in Santiago. This work has been supported by FONDECYT 1130354, CONICYT FONDECYT Postdoctorado 3140550, ACT127 and European Space Agency Topical Team on granular materials No. 4000103461.

[1] A. N. Kolmogorov, Dokl. Akad. Nauk SSSR **32**, 19 (1941); reprinted in Proc. R. Soc. Lond. A **434**, 15 (1991).
[2] U. Frisch, *Turbulence: The Legacy of A. N. Kolmogorov* (Cambridge University Press, New York, 1995).
[3] A. Mehta, *Granular Physics* (Cambridge University Press, New York, 2007).
[4] I. Aranson and L. Tsimring, *Granular Patterns* (Oxford University Press, New York, 2009).
[5] S. Aumaître, S. Fauve, S. McNamara, and P. Poggi, Euro. Phys. J. B **19**, 449 (2001).
[6] S. Aumaître, J. Farago, S. Fauve, and S. Mc Namara, Euro. Phys. J. B **42**, 255 (2004).
[7] N. Garnier and S. Ciliberto, Phys. Rev. E **71**, 060101 (2005).
[8] C. Falcón and E. Falcon, Phys. Rev. E **79**, 041110 (2009).
[9] M. Bonaldi *et al.*, Phys. Rev. Lett. **103**, 010601 (2009).
[10] G. Alhers, S. Grossman, and D. Lohse, Rev. Mod. Phys. **81**, 503 (2009).
[11] M. M. Bandi and C. Connaughton, Phys. Rev. E **77**, 036318 (2008).
[12] O. Cadot, C. Touzé, and A. Boudaoud, Phys. Rev. E **82**, 046211 (2010).
[13] E. Falcon, S. Aumaître, C. Falcón, C. Laroche, and S. Fauve, Phys. Rev. Lett. **100**, 064503 (2008).
[14] U. Seifert, Rep. Prog. Phys. **75**, 126001 (2012).
[15] S. Ciliberto, S. Douady, and S. Fauve, Europhys. Lett. **15**, 23 (1991).
[16] R. Zwanzig, *Nonequilibrium Statistical Mechanics* (Oxford University Press, New York, 2001).
[17] R. Kubo, M. Toda, and N. Hashitsume, *Statistical Physics II: Nonequilibrium Statistical Mechanics*, Springer Series in Solid-State Sciences (Springer, New York, 1985).
[18] P. Pieranski, J. Physique **44**, 573 (1983).
[19] J. M. Luck and A. Mehta, Phys. Rev. E **48**, 3988 (1993).
[20] J.-C. Geminard and C. Laroche, Phys. Rev. E **68**, 031305 (2003).
[21] S. Giusepponi, F. Marchesoni, and M. Borromeo, Physica A **351**, 142 (2005).
[22] C. R. de Oliveira and P. S. Goncalves, Phys. Rev. E **56**, 4868 (1997).
[23] T. W. Burkhardt and S. N. Kotsev, Phys. Rev. E **73**, 046121 (2006).
[24] E. Falcon, C. Laroche, S. Fauve, and C. Coste, Eur. Phys. J. B **5**, 111 (1998).
[25] R. P. Chhabra, S. Agarwal, and K. Chaudhary, Powder Technol. **129**, 53 (2003).
[26] C. Craig, Ann. Math. Stat. **7**, 1 (1936).
[27] R. Hogg, E. Tanis, and D. Zimmerman, *Probability and Statistical Inference* (Pearson, New York, 2001).
[28] S. Aumaître, *Fluctuations and Instabilities in Out-of-Equilibrium Systems* (Habilitation à diriger les recherches (HDR), École Normale Supérieure de Lyon, 2014).
[29] A. Pumir, Phys. Fluids **8**, 3112 (1996).
[30] S. Cerutti and C. Meneveau, Phys. Fluids **10**, 928 (1998).
[31] X.-D. Shang, X.-L. Qiu, P. Tong, and K.-Q. Xia, Phys. Rev. Lett. **90**, 074501 (2003).
[32] O. Shiskina and C. Wagner, Phys. Fluids **90**, 085107 (2007).
[33] W. L. Shew, Y. Gasteuil, M. Gibert, P. Metz, and J. F. Pinton, Rev. Sci. Inst. **78**, 065105 (2007).
[34] D. J. Evans, E. G. D. Cohen, and G. P. Morriss, Phys. Rev. Lett. **71**, 2401 (1993).